Viscosity and transient electric birefringence study of clay colloidal aggregation

Audun Bakk* and Jon O. Fossum
Department of Physics, Norwegian University of Science and Technology, NTNU, NO-7491 Trondheim, Norway

Geraldo J. da Silva†
Physics Institute, University of Brasília, Caixa Postal 04513, 70919-970 Brasília Distrito Federal, Brazil

Hans M. Adland, Arne Mikkelsen, and Arnljot Elgsaeter
Department of Physics, Norwegian University of Science and Technology, NTNU, NO-7491 Trondheim, Norway
(Received 30 May 2001; revised manuscript received 10 September 2001; published 23 January 2002)

We study a synthetic clay suspension of laponite at different particle and NaCl concentrations by measuring stationary shear viscosity and transient electrically induced birefringence (TEB). On one hand the viscosity data are consistent with the particles being spheres and the particles being associated with large amount bound water. On the other hand the viscosity data are also consistent with the particles being asymmetric, consistent with single laponite platelets associated with a very few monolayers of water. We analyze the TEB data by employing two different models of aggregate size (effective hydrodynamic radius) distribution: (1) bidisperse model and (2) log-normal distributed model. Both models fit, in the same manner, fairly well to the experimental TEB data and they indicate that the suspension consists of polydisperse particles. The models also appear to confirm that the aggregates increase in size vs increasing ionic strength. The smallest particles at low salt concentrations seem to be monomers and oligomers.

DOI: 10.1103/PhysRevE.65.021407 PACS number(s): 82.70.Dd, 78.20.Fm, 61.20.Lc, 66.20.+d

I. INTRODUCTION

Laponite [1–4] is a widely studied synthetic clay that belongs to the family of swelling 2:1 clays [5]. All dehydrated clays have a layered silicate mesostructure. The 2:1 clays (or smectites) thus consist of 1 nm thick and charged (negative surface charge and a smaller positive edge charge) mesosheets, which in the dehydrated state stack (like decks of cards) by sharing charge-compensating cations. Laponite is a particularly interesting model system because of the merely monodisperse size of the colloidal platelets (25–30 nm diameter, see Fig. 1). This is different from natural and other synthetic clays, which in general have a polydisperse distribution of micrometer sized platelets. Introductions describing the crystallographic structures and providing precise definitions of both natural and synthetic clays, including laponite (a synthetic hectorite), may be found in several books [5,6].

The addition of salt-containing water to these mesoscopic platelet systems gives rise to interesting colloidal dispersion ''phase'' diagrams. Four separate regions (phases) of physical complexity have been suggested from experimental observations of clay-electrolyte-concentration diagrams of laponite: isotropic liquid (IL), isotropic gel (IG), nematic gel, and flocculation [2].

Traditional theory of Derjaguin, Landau, Verwey, and Overbeek [7,8], where both van der Waals and double-layer forces are considered, provides the simplest available model capable of describing this complex behavior. Transitions and aggregate structures within stable phases may thus be discussed in terms of an interaction potential between individual platelets. This is achieved by adding the electrolyte-independent van der Waals attraction and the double-layer repulsion as characterized by an electrolyte-concentration-dependent Debye screening length [9]. The sum of these two forces yields different local potential minima, with regard to platelet-platelet interactions, which may be changed by varying the ionic strength.

The IL phase is a suspension of Brownian particles, and is made up of single platelets and/or larger aggregates of several laponite platelets suspended in water. The size and compactness of these aggregates may depend on electrolyte concentration via the Debye screening length. The aggregates in this phase are, in general, too small to scatter visible light appreciably, thus yielding a transparent liquid with a viscosity that may be changed by varying the salt-clay concentration. This phase can be made birefringent by applying high electric fields, as will be evident from the present work. At low concentrations the liquid seems to be Newtonian, whereas upon approaching the IL-IG line the IL phase can display non-Newtonian and thixotropic behavior. The aggre-

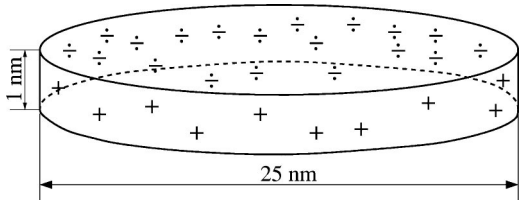

FIG. 1. Schematic illustration that shows the geometry and dimensions of a laponite platelet. The surface charges are indicated by negative charges (÷) and smaller positive charges (+) at the edges.

*Corresponding author.
Email address: Audun.Bakk@phys.ntnu.no
†Present address: Department of Physics, Norwegian University of Science and Technology, NTNU, NO-7491 Trondheim, Norway.

gate structure becomes a gel when the clay concentration becomes sufficiently large [4], possibly signaling a glass transition [10].

In the present paper we report on experimental studies of laponite samples within the low clay-concentration regime, i.e., in the IL phase. We study samples at different clay and NaCl concentrations by means of two techniques, viscometry, thus measuring the effective hydrodynamic volume of the suspended particles, and by transient electric induced birefringence (TEB) measurements, thus obtaining information about rotational diffusion. Combining our data from these two techniques we attempt to extract information about shape and size distribution of the laponite aggregates in the IL phase. The TEB technique is widely used in studying the rotational motion of macromolecules in solution [11], and has also been used for studying natural clays [12].

The goal of the present study is twofold: (1) extract information about aggregate volumes and shapes in laponite suspensions, and (2) investigate the possibilities and limitations of using TEB measurements combined with viscometry in order to characterize such complex colloid aggregate systems.

The paper is organized as follows: Section II gives a short introduction to intrinsic viscosity and in Sec. III we discuss some general aspects of rotational diffusion and birefringence. In Sec. IV we present the sample preparation and the experimental setup, and in Sec. V we discuss the experimental data from the viscosity and the TEB measurements in view of two different models with regard to the distribution of the aggregate sizes. Section VI is a summary.

II. INTRINSIC VISCOSITY OF RIGID PARTICLES

The *intrinsic viscosity* is defined as [13]

$$[\eta]=\lim_{c\to 0}\frac{\eta_{\mathrm{rel}}-1}{c}, \tag{1}$$

where c is the laponite concentration, and the relative viscosity equals

$$\eta_{\mathrm{rel}}=\frac{\eta'}{\eta}, \tag{2}$$

where η' is the macroscopic viscosity (water and laponite) and η is the water viscosity. Eq. (2) can be linearized to

$$\eta_{\mathrm{rel}}=1+[\eta]c, \tag{3}$$

which obviously has the correct limit of zero laponite concentration, where $\eta_{\mathrm{rel}}=1$.

It can be shown that $[\eta]$ for a compact macromolecule or aggregate of arbitrary shape can be described by the heuristic expression [13,14]

$$[\eta]=\nu(\delta\overline{V}_1+\overline{V}_2), \tag{4}$$

where ν is the dimensionless Simha factor containing all the shape dependence. The parameters $\overline{V}_1$ and $\overline{V}_2$ are the partial specific volumes of water (1.0 cm^3/g) and solute, respectively. The $\overline{V}_2$ is the change in solution volume per unit solute mass added, at the limit of zero solute concentration. The δ is the hydration ratio i.e., δ grams of bound water per gram solute (aggregate).

The Simha factor in Eq. (4) equals 2.5 for a sphere and increases with increasing asymmetry, i.e., $\nu\geqslant 2.5$. For the Laponite used in this present study $\overline{V}_2=0.37\,\mathrm{cm}^3/\mathrm{g}$. A change in $[\eta]$ can then arise as the result of a change in ν, changed hydration factor δ, or a combination of such changes. However, if the particle geometry is known, and $\overline{V}_1$ and $\overline{V}_2$ in Eq. (4) are known, the intrinsic viscosity is thus implicitly a measure of the hydration of the particles (aggregates).

It should be noted that it is not possible to determine the size of the particles only from a intrinsic viscosity measurement. For example, a mixture of spheres with different sizes will give the same $[\eta]$ as a monodisperse solution of spheres, provided that the hydration ratios of the spheres in the two cases are the same.

III. BIREFRINGENCE OF RIGID PARTICLES

When no external forces influence the orientation of the particles, they will be randomly oriented and in thermodynamic equilibrium. If the particles for some reason have a specific orientation at a given time, thermal (Brownian) motion will make the system decay to this equilibrium. It can be shown that the birefringence relaxation time of a dilute solution of identical particles, can have as many as five relaxation times [15]. All these decay times are known functions of the rotational mobility tensor [15,16], but for most particle geometries it is not possible, using experimental data, to obtain reliable estimates of more than two decay times.

In the analysis of the TEB data we will restrict ourselves to models with geometries that makes it adequate to use only one decay time. To induce the birefringence it is common to use electric field pulses that are rectangular as function of time, but in order to analyze the properties of the particle electric dipoles it is also useful to employ double pulses where the electric field of the second pulse is reversed relative to the first pulse [17,18].

In the case when the system is dominated by two distinct types of particles, i.e., a *bidisperse* model, each type of particles may have its own relaxation time. The birefringence signal at time t can then be described by

$$\frac{\Delta n(t)}{\Delta n(0)}=a_1\exp\left(-\frac{t}{\tau_1}\right)+a_2\exp\left(-\frac{t}{\tau_2}\right), \tag{5}$$

where $\Delta n(0)$ is the birefringence at time $t=0$, and a_1 and a_2 represent the relative contribution to the total birefringence from each of the two particle types, respectively. This model is used in Sec. V B. However, Eq. (5) can also be interpreted as representing a system of monodisperse anisotropic particles for which the five relaxation times of the particles is reduced to two times because of the particle symmetry.

For a rigid body, with one axis of rotational symmetry, the birefringence relaxation time is given by $\tau=(6D^{(\mathrm{rot})})^{-1}$

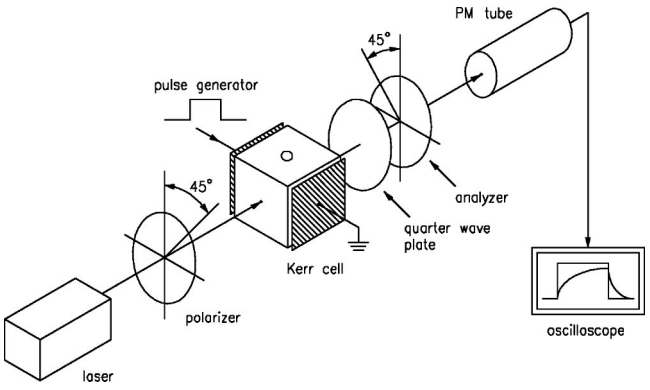

FIG. 2. Schematic illustration of the TEB experimental setup. Brief description in Sec. IV C; for further details see, e.g., Refs. [17,18,25].

[15,16], where $D^{(\mathrm{rot})}$ is the macroscopic rotational diffusion coefficient. The Nernst-Einstein relation [19], valid for dilute solutions, relates $D^{(\mathrm{rot})}$ to the rotational friction tensor $\zeta^{(\mathrm{rot})}$ [20]

$$D^{(\mathrm{rot})}=\frac{k_B T}{\zeta^{(\mathrm{rot})}}, \tag{6}$$

where k_B is the Boltzmann constant and T is the absolute temperature. The rotational friction for a sphere of radius r_s equals $\zeta_s^{(\mathrm{rot})}=8\pi\eta r_s^3$ [13], where η is the viscosity of water. This yields a birefringence relaxation time

$$\tau=\frac{\zeta^{(\mathrm{rot})}}{6k_B T}=\frac{4\pi\eta}{3k_B T}r_s^3. \tag{7}$$

Equation (7) relates the birefringence relaxation time to the effective hydrodynamic radius for rotation of a sphere.

IV. EXPERIMENT

A. Sample preparation

Laponite RD powder as purchased from Laporte Absorbents (UK), was added to NaCl containing water. The *p*H in the salt-water was adjusted to 10 before addition of laponite powder in order to prevent decomposition of the platelets themselves [2,21]. The samples were then stirred for two days, using a magnetic stirrer, before each sample was placed in a sample tube. Small sample portions were then taken from the tubes and the experiments reported here were performed. All investigated samples were 1–1.5 months old, with two exceptions. Samples AA and AB discussed below were both 6 months old.

It is important to note that laponite suspensions are known to show slow long-term aging effects [22]. This is probably due to decomposition of individual platelets, and thereby disintegration of the aggregates, when the suspension samples are not sealed from air. Such scaling was not carried out for the present samples. The effect of aging is, therefore, expected to be significant for the aggregates characterized here. Nevertheless, our samples were prepared and stored in a repeatable manner.

The present samples were not filtered, as was done and emphasized recently by Nicolai and Cocard [21] for their light scattering studies. Our samples could thus contain some large impurities reported in some cases to dominate static light scattering experiments [21], but both TEB and viscosity measurements are less sensitive to such impurities than static light scattering.

B. Viscometer

The viscosity was measured using a rotational conicylindrical viscometer (CONTRAVES Low Shear 30) with a *Couette* geometry, which consists of a static rod, measuring the torque, in a concentric rotating cup filled with the suspension. For a further introduction to the instrumental setup and the theoretical aspects of the rheology, see e.g., Van Wazer *et al.* [23]. The temperature in the suspension was fixed to 20 °C throughout the experiment by a thermostat (Haake D8). The torque signal from the rod was sampled and transformed to viscosity by a instrumentation data program (LABVIEW) [24].

C. TEB setup

The setup for the TEB instrument is shown in Fig. 2. The light source is an argon laser (Omnichrome 543-AF) operated at wavelength 488 nm. The monochromatic light is polarized at an angle of 45°, relative to the electric field, and passes through the Kerr cell where the sample is located. In the Kerr cell the aggregates are exposed to a pulsed electric field in the horizontal direction (see Fig. 2). The distance between the parallel electrodes is 4 mm. The optical anisotropy caused by the electric field makes the light exiting the Kerr cell, temporally, elliptically polarized.

When the principal axis of the analyzer is oriented perpendicular to the polarizer, the light intensity measured by the photomultiplicator (PM) is proportional to the square of the birefringence Δn (quadratic detection). The PM voltage is displayed on a digital storage oscilloscope (Tektronix TDS 620).

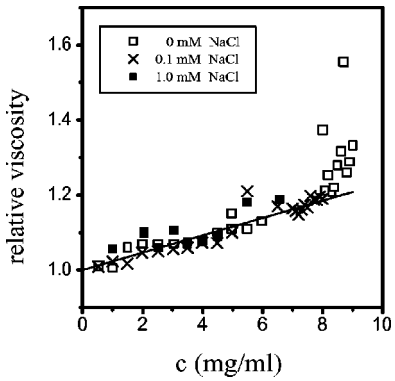

FIG. 3. Relative viscosity [see Eq. (2)] vs laponite weight concentration at three different NaCl concentrations. The concentration parameter c is weight laponite per unit volume of water. The straight line corresponds to a linear least-squares fit of the linear interval of the relative viscosity $\eta_{\mathrm{rel}}=1+0.23c$.

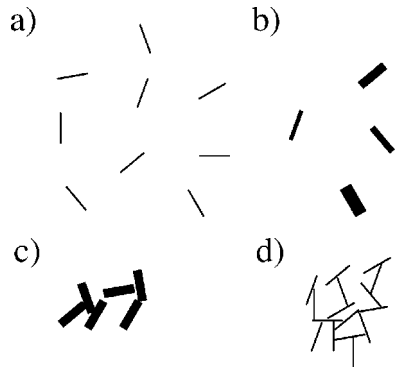

FIG. 4. Schematic examples of different models of laponite particle association. The different models shown are (a) dispersed suspension that consists of noninteracting single laponite platelets, (b) noninteracting stacks of platelets, (c) interacting stacks of platelets, and (d) ''house of cards'' configuration. For a further discussion of the different models see, e.g., van Olphen [5].

The temperature in the Kerr cell was fixed to 20 °C throughout the experiment by a thermostat (Haake D8). During the experiment the temperature was checked by a platinum thermometer. The temperature rise was found to be about 0.8 °C after a typical series of six pulses with 0.25 ms pulse length, 2.5 s intervals, and using an applied voltage of 850 V.

For further technical details on TEB experiments see Ref. [17,18,25].

V. DISCUSSION

A. Viscosity

In Fig. 3 we plot the relative viscosity [see Eq. (2)] vs the laponite concentration for three different NaCl concentrations (0, 0.1, and 1.0 mM). At low laponite concentrations ($c<8$ mg/ml) one sees a typical linear dependence of the relative viscosity, while for large Laponite concentrations ($c>8$ mg/ml) it raises abruptly. The latter is possibly due to a onset of gelation of the clay suspension [2]. In the linear regime we do a linear least-squares fit, where the inclination of the relative viscosity equals the intrinsic viscosity [see Eq. (3)]. We thus obtain $[\eta]=23\pm1\ \mathrm{cm}^3/\mathrm{g}$ for 0 and 0.1 mM [NaCl], and $[\eta]=26\pm3\ \mathrm{cm}^3/\mathrm{g}$ for 1.0 mM [NaCl]. As the difference is small between the various salt concentrations we obtain the value

$$[\eta]=23\pm1\ \mathrm{cm}^3/\mathrm{g}, \tag{8}$$

based upon the linear part of the relative viscosity data at all salt concentrations.

We may define a critical particle concentration c^* where there is one platelet per cube with side lengths that equals 25 nm, i.e., the diameter of a laponite platelet, and these cubes occupy the entire volume. This yields $c^*\approx85$ mg/ml. In the present experiments the largest Laponite concentration is 8 mg/ml, i.e., $c\ll c^*$.

One difficulty associated with using Eq. (4) is that we do not know the value of δ, because the hydration depends of the geometry of the associated particles. This association will again depend upon the laponite concentration and the ionic strength of the solution. Figure 4 gives examples of different models of particle association. The ''house of cards'' configuration in Fig. 4(d) has likely a large δ compared to, e.g., the single platelets in Fig. 4(a).

Assuming a spherical shape of the aggregates, the Simha factor ν in Eq. (4) equals 2.5, as stated in Sec. II. Inserting $[\eta]=23\ \mathrm{cm}^3/\mathrm{g}$, $\nu=2.5$, $\overline{V_1}=1.0\ \mathrm{cm}^3/\mathrm{g}$, and $\overline{V_2}=0.37\ \mathrm{cm}^3/\mathrm{g}$ into Eq. (4), yields a hydration ratio $\delta=8.8$, i.e., 8.8 g of water per gram of laponite platelets. The laponite platelet has a density 2.7 g/cm^3, thus $\delta=8.8$ yields that the hydrated water volume, associated to each laponite platelet, is on average approximately 24 times the volume of a platelet. In other words, the viscosity experiment, based upon a spherical geometry of the aggregates, shows that aggregates are associated with a large amount of water. The latter may indicate a kind of ''house of card'' [5] association of the platelets, as shown in Fig. 4(d), but we stress that this conclusion may be an artifact due to the assumed spherical shape of the aggregates.

In light of the measured intrinsic viscosity $[\eta]=23\ \mathrm{cm}^3/\mathrm{g}$ [see Eq. (8)], it is interesting to compare this to that of an aggregate system where each platelet *on average* occupies a cylindrical volume with diameter and height equivalent to its own volume, i.e., 25 nm. This means that one laponite platelet (see Fig. 1) is associated with a water volume that is 24 times its own volume, which is the same estimate as obtained from the spherical approximation used above.

However, the source of the intrinsic viscosity described by Eq. (4) may also be an asymmetric shape of the particles, which will give a larger Simha factor [13] and consequently a smaller hydration ratio δ in Eq. (4). Thus, asymmetry implies a more dense packing of the aggregates compared to spherical aggregates, when a constant intrinsic viscosity is assumed.

Assuming an asymmetric particle shape is further motivated by, e.g., Avery and Ramsay [26], Rosta and von Gunten [27], and Nicolay and Cocard [21] who concluded that the smallest particles in a laponite suspension were monomers [21,26] and/or oligomers [21,27]. In this respect it is interesting to investigate the maximum asymmetry that is reconcilable with a ''realistic'' minimum of hydration. We assume a monolayer of water molecules with thickness 2.5 Å around each laponite platelet, independent of whether it is single or in an aggregate. This gives a hydration ratio $\delta=0.2$. Inserting this $\delta=0.2$ into Eq. (4) implies a Simha factor $\nu=40$, which corresponds to an axial ratio 25 for an oblate ellipsoid [13]. This is interesting because an axial ratio 25 is approximately the ratio between the diameter and thickness of a single laponite platelet, which indeed can be approximated by an oblate ellipsoid.

Thus, the viscosity experiment does not exclude the possibility that the suspension consists of oblate particles that have axial ratios up to around 25, e.g., laponite monomers.

B. Bidisperse model (model 1)

The experimental TEB data for four different samples are shown in Fig. 5. It is assumed that the fluctuations of the data

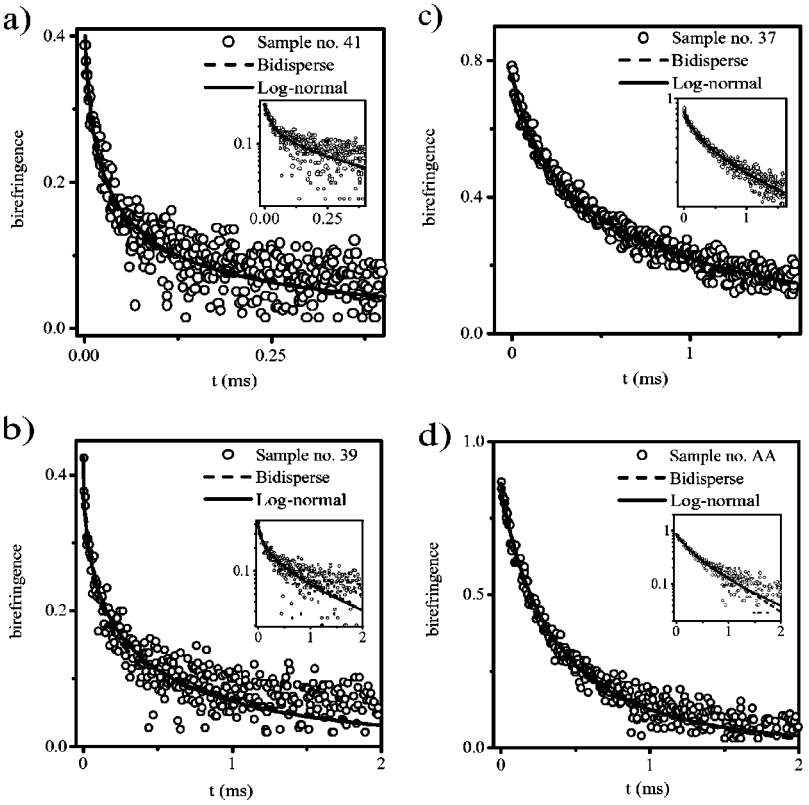

FIG. 5. Birefringence vs time t for four different samples. The experimental data are fitted by studying two different models: the bidisperse model in Sec. V B and the log-normal model in Sec. V C. The corresponding parameters are listed in Tables I and II. Note that for the inserted plots the axis of the birefringence is logarithmic, while the t-axis is linear.

in the TEB experiment are the a result of instrument noise, and not intrinsic to the samples. One source of error is the PM tube with an absolute error of ± 0.05 V. This will make the analysis for large times, where the relaxation signal is small, uncertain. The error estimates of the least-squares fit for the bidisperse model and log-normal model are presented in Table I and II, respectively.

The simplest possible fit to the TEB data is obtained by using two exponential functions with different birefringence decay times as in Eq. (5). The two relaxation times τ_1 and τ_2, correspond to two effective hydrodynamic radii r_1 and r_2, respectively. We have assumed a spherical aggregate geometry. The relation between τ and r for a sphere is given in Eq. (7). The obtained parameter estimates are presented in Table I. We find that increase of the salt concentration results in longer relaxation times, as seen in Table I.

We note from Table I that the standard deviation is small, despite the relatively large instrument error. This is probably due to the large amount of data available for each sample. However, samples numbers 28 and 29 exhibit a large standard deviation of the parameter r_2, but note that the corresponding amplitudes a_2 are small.

We now look at the shortest relaxation times at low salt concentrations ($[\mathrm{NaCl}] \leqslant 0.1$ mM). For spherical particles this corresponds to a mean value $\langle r_1 \rangle = 23$ nm. It would be interesting to calculate the corresponding size of a particle with an axial ratio that corresponds to a hydrated laponite platelet. If we assume one monolayer of water with thickness 2.5 Å attached to the platelet with diameter 25 nm and height 1 nm, this corresponds to an hydration axial ratio $p \approx 17$. Employing data given in Ref. [13] we find that the diameter of this particle is about 30 nm if we assume the shape to be that of an oblate ellipsoid.

By doing the same analysis as in the previous paragraph and using $p = 25$, which was the largest possible asymmetry calculated from the viscosity experiment, we also get a diameter around 30 nm. Thus, from the viscosity experiment together with the fit of the bidisperse model to the TEB data we may conclude that the smallest particles in the suspension have diameters in the range 20–35 nm, and that the diameter increases with increasing asymmetry of the particles. If we further assume that the individual platelets do not decompose, we conclude that the smallest particles at low salt content are individual platelets as Avery and Ramsay [26], and Nicolay and Cocard [21] concluded.

It is interesting to note that the effective hydrodynamic radius for the smallest aggregates are approximately one half of the larger ones for the corresponding pairs, i.e., $r_2/r_1 \approx 2$ in Table I. This means that we have some small aggregates and some large aggregates. Figure 5 shows the parameter fitting for some of the sample data. The fit is satisfactory in view of the simplicity of the model. However, it is more realistic to expect a *distribution* of the particle sizes. In the next section we will show that the TEB data also can be approximated by a log-normal distribution.

C. Log-normal distributed model (model 2)

The exponential fits in the preceding section suggest that there may be a broad distribution of the colloid particle size for some of the samples. Next we, therefore, tried to fit the TEB data, with regard to the size of the aggregates, onto a

TABLE I. Parameters associated with the various samples when a sum of two exponential decays is used (model 1). Parameters τ_i and r_i are the corresponding pairs of the relaxation times and the effective hydrodynamic radii, respectively, a_2/a_1 is the amplitude ratio of the birefringence, r_m is the weighted mean of r_1 and r_2, c equals mass laponite per unit volume of water, and [NaCl] is the salt concentration. The standard deviation (SD) is written as ±SD.

Sample	τ_1 (μs)	r_1 (nm)	τ_2 (μs)	r_2 (nm)	a_2/a_1	r_m (nm)	c (mg/ml)	[NaCl] (mM)
21	3.8	16 ±1	55	37 ±2	1.3	28	1.0	0
20	2.4	13 ±1	40	33 ±1	1.4	25	1.5	0
18	2.5	13 ±1	50	36 ±2	0.67	22	2.5	0
11	68	40 ±2	240	62 ±2	1.5	53	6.0	0
41	24	29 ±1	320	68 ±2	0.58	43	8.0	0
30	55	37 ±7	200	58 ±3	3.2	53	1.0	0.1
29	14	25 ±1	1010	99 ±20	0.20	37	1.5	0.1
28	8.2	20 ±1	850	94 ±94	0.11	18	2.0	0.1
27	2.3	13 ±1	59	39 ±3	0.35	20	2.5	0.1
AB	29	30 ±2	390	72 ±2	2.1	58	2.5	0.5
39	97	46 ±2	1170	100 ±2	0.85	71	1.0	1.0
38	57	37 ±1	790	92 ±3	0.58	57	1.5	1.0
37	82	43 ±1	650	86 ±1	1.7	70	2.0	1.0
AA	140	52 ±3	680	88 ±1	1.8	75	2.5	4.0

Gaussian distribution, but we found that this did not work well in general. However, we found that the TEB data fit well onto a log-normal distribution, with regard to the radius of the aggregates. The log-normal probability distribution of a quantity r, with mean r_s, and standard deviation σ reads

$$p(r)=\frac{1}{\sqrt{2\pi}\sigma r}\exp\left(-\frac{\ln^2(r/r_s)}{2\sigma^2}\right), \tag{9}$$

which is asymmetric and has a longer tail than the normal distribution, as shown in Fig. 6. It should also be noted that the Gaussian distribution is somewhat unphysical in light of a probability larger than zero for $r<0$, in contrast to the log-normal distribution that is only defined for $r\geqslant 0$.

The log-normal distribution was fitted to the square root of the voltage from the PM, which is proportional to the birefringence $\Delta n(t)$, where t is the time. When we assume an exponential decay of the birefringence, aggregate radius r, and relaxation time τ_s, the birefringence reads

$$\Delta n(t)\sim\int_0^\infty dr\, p(r)e^{-t/\tau_s}, \tag{10}$$

and τ_s is the birefringence relaxation time for a sphere (s). The τ_s is given by letting $\tau\rightarrow\tau_s$ in Eq. (7).

The parameter fit is presented in Table II, from which it is clear that we have in general, a broad particle size distribution, i.e., large standard deviations σ. In Fig. 5 we see that the log-normal approximation is almost equivalent to the bidisperse model for these samples, with regard to the fit to the TEB data.

An interesting observation was that for sample number 39, an applied Kerr cell voltage of 850 V for 0.5 ms was not enough to align the aggregates, because the birefringence signal seemed not to be saturated at $t=0$, i.e., when the electric field was switched off. If we applied the same voltage for 1.5 ms the birefringence amplitude became saturated at $t=0$. However, the relaxation birefringence signal (after $t=0$) associated with a pulse length of 1.5 ms applied to sample number 39 appears to be almost equivalent to the birefringence signal associated with a pulse length of 0.5 ms. Nevertheless, it would in a future experiment be interesting to investigate the samples using different applied voltages and pulse lengths, which effectively can act as a particle filter.

It is worth noting that the log-normal distribution has also been applied to describe the polydispersity of the diameters of magnetic cores in ferrofluids [28]. Furthermore, Ivanov [29] showed that the continuous behavior of this particle distribution can be substituted by a bidisperse model, when the majority of the particles have the smaller radius.

One source of error in the experiments reported here is that we do not know whether the rotational motion of the aggregates in the Couette geometry deform the aggregates permanently, and thus giving rise to another configuration than before the experiment. In future experiments it would be interesting to first test the samples in the TEB device, whereupon one should measure the viscosity, and finally put the sample back into the TEB device in order to check the influence of the flow on the aggregates in the viscometer. It might also be interesting to check flow induced birefringence in order to investigate the latter effect.

The log-normal distribution for four different samples is drawn in Fig. 6, all showing the characteristic long tail. Because these distributions yielded the best fit to the TEB data, this may tell us that the samples have some large aggregates that make the distribution asymmetric compared to a Gaussian distribution [21]. In Fig. 6 we also see the effect of a relatively small standard deviation for sample number *AA* ($\sigma=0.24$), where in this particular case the log-normal distribution could be approximated by a normal distribution. We note for the log-normal distributed model, as for the bidisperse model, that for some of the samples the fit to experimental data for long times is only fair. Thus, we cannot rule out the presence of some large particles which we are not able to account for within our present models.

TABLE II. Parameters associated with the log-normal distribution (model 2). Parameter r_s is the mean value of the effective hydrodynamic radius, with a standard deviation σ. Parameters c and [NaCl] are explained in Table I. The standard deviation (SD) is written as $\pm$SD.

Sample	r_s (nm)	σ	c (mg/ml)	[NaCl] (mM)
21	24±2	0.71±0.09	1.0	0
20	23±1	0.65±0.06	1.5	0
18	17±1	0.73±0.03	2.5	0
11	52±1	0.23±0.01	6.0	0
41	33±2	0.70±0.05	8.0	0
30	53±1	0.18±0.03	1.0	0.1
29	32±4	0.7±0.1	1.5	0.1
28	27±4	0.9±0.2	2.0	0.1
27	14±1	0.72±0.04	2.5	0.1
AB	61±2	0.61±0.08	2.5	0.5
39	80±5	0.7±0.1	1.0	1.0
38	56±1	0.44±0.02	1.5	1.0
37	71±1	0.46±0.02	2.0	1.0
AA	75±1	0.24±0.02	2.5	4.0

The large standard deviation seen in Table II indicates that we have a polydisperse particle size distribution. This is substantiated by a look at the amplitude ratios in Table I, which fluctuates around 1 and where the corresponding pairs of radii have a ratio around 2. Thus, we come to the same conclusion as Nicolay and Cocard [21] in their static and dynamic light scattering experiments, i.e., that the laponite particles are polydisperse. Here we note that Rosta and von Gunten [27] come to the opposite conclusion, i.e., that the suspension is more or less monodisperse.

VI. SUMMARY AND CONCLUSION

We study a laponite clay suspension at different laponite and salt concentrations by shear viscometry and by TEB measurements. This is to the authors' knowledge the first reported TEB study of laponite. Two different models of the distribution of the aggregate sizes are considered: (1) bidisperse model and (2) log-normal distributed model.

The viscosity data show, when assuming that the aggregates are spherical, that we have a ''house of cards'' [5] association of the laponite platelets, i.e., the aggregates are associated with a large amount of hydrated water. However, the viscosity data may also be interpreted as being due to asymmetrical aggregates with a smaller hydration ratio than the spherical aggregates. In this respect we show that it is possible to interpret the viscosity data as oblate ellipsoidal

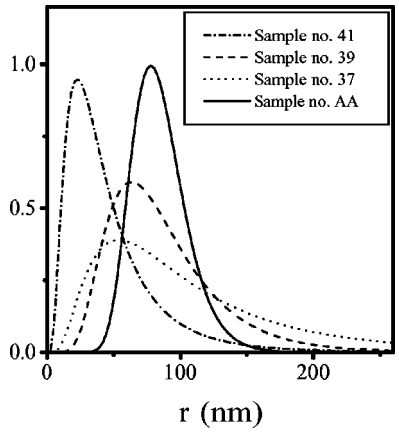

FIG. 6. Log-normal distribution of the samples that correspond to Fig. 5, where r is the effective hydrodynamic radius of the aggregates. The distribution has been normalized to unity.

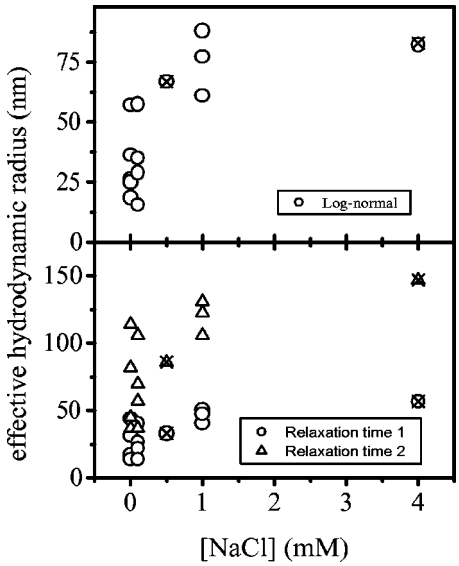

FIG. 7. Effective hydrodynamic radius for the log-normal distributed model of the aggregate sizes in the upper plot, and the effective hydrodynamic radius for the bidisperse model associated with the two relaxation times τ_1 and τ_2 in the lower plot. Data from Tables I and II are used. The experimental data points with ''×'' correspond to samples *AA* and *AB*, which were 6 months old, as stated in Sec. IV A.

particles with an asymmetry up to 25, e.g., single laponite platelets.

The two models were fitted to experimental data obtained using TEB technique, and the models seem to fit the experimental data fairly well in most cases. This means, for the samples studied, that the simplistic bidisperse model is almost equivalent to the log-normal distribution. Most of the samples show, in view of the log-normal model, that we have a broad particle size distribution. This is the same conclusion as Nicolay and Cocard [21], and the opposite of Rosta and von Gunten [27], who performed light scattering experiments. However, from the available data it cannot be ruled out that the apparent lack of fits, for some long time tails, may suggest a particle size distribution that includes some larger laponite aggregates that cannot be covered within our present models.

Both models show that the aggregates increase in size, from a hydrodynamic point of view, when the salt concentration is increased, as seen in Fig. 7. Furthermore, our present experiments do not confirm or rule out the possibility of a correlation between particle size and laponite concentration. The smallest particles in the suspensions consist of only one or a very few laponite platelets at low salt concentrations, as also Avery and Ramsay [26], Rosta and von Gunten [27], and Nicolay and Cocard [21] concluded.

Finally we note that the present laponite samples were not made, filtered, or stored (scaled from air) in the same controlled manner as recent light scattering studies by Nicolai and Cocard [21].

In a future work it would be important to prepare the samples in a different way and also to study other synthetic clay suspensions such as fluorohectorite. In light of the broad asymmetric tails of the log-normal distribution for most of the samples reported here, it would be of considerable interest and importance to study suspension samples for which the large aggregates are filtered out successively.

ACKNOWLEDGMENTS

The authors would like to thank L. Wohlen for the drawing of Fig. 2. A.B. and J.O.F. thank NTNU/NFR SUP 115185/420 for financial support during the first part of the work. A.B. thanks the Research Council of Norway for financial support (Contract No. 129619/410) in the latter part of the work. H.M.A. thanks the Department of Physics, NTNU, for financial support. G.J. da S. acknowledges the Conselho Nacional de Desenvolvimento Científico e Tecnológico (CNPq/Brazil) for financial support.

[1] J.-O. Fossum, in *Soft Condensed Matter: Configurations. Dynamics, and Functionality*, edited by A. T. Skjeltorp and S. F. Edwards (Kluwer Academic, Netherlands, 2000), p. 269, and references therein.

[2] A. Mourchid, E. Lecolier, H. VanDamme, and P. Levitz, Langmuir **14**, 4718 (1998).

[3] J. P. C. Gabriel, C. Sanchez, and P. Davidson, J. Phys. Chem. **100**, 11 139 (1996).

[4] S. Cocard, J. F. Tassin, and T. Nicolai, J. Rheol. **44**, 585 (2000), and references therein.

[5] H. van Olphen, *An Introduction to Clay Colloid Chemistry*, 2nd ed. (Krieger Publishing Company, Florida, 1991).

[6] B. Velde, *Introduction to Clay Minerals* (Chapman and Hall, London, 1992).

[7] B. V. Derjaguin and L. Landau, Acta Physicochim. URSS **14**, 633 (1941).

[8] E. J. W. Verwey and J. T. G. Overbeek (with the collaboration of K. van Nes), *Theory of the Stability of Lyophobic Colloids: the Interaction of Sol Particles Having an Electric Double Layer* (Elsevier, New York, 1948).

[9] J. N. Israelachvili, *Intermolecular and Surface Forces*, 2nd ed. (Academic, London, 1992).

[10] D. Bonn, J. Tanaka, G. Wegdam, H. Kellay, and J. Meunier, Europhys. Lett. **45**, 52 (1999).

[11] P. J. Hagerman, Curr. Opin. Struct. Biol. **6**, 643 (1996); C. Houssier, Colloids Surf., A **148**, 3 (1999); R. Sasai, N. Ikuta, and K. Yamoaka, J. Phys. Chem. **100**, 17 266 (1996); J. K. Phalakornkul, A. P. Gast, and R. Pecora, Macromolecules **32**, 3122 (1999); F. Charney, Q. Rev. Biophys. **21**, 1 (1988).

[12] I. C. Hinds, P. J. Ridler, and B. R. Jennings, Clay Miner. **31**, 549 (1996).

[13] C. R. Cantor and P. R. Schimmel, *Biophysical Chemistry* (Freeman, San Francisco, 1980), Vol. II, Chaps. 10 and 12.

[14] A. Bakk, Phys. Rev. E **63**, 061906 (2001).

[15] W. A. Wegener, R. M. Dowben, and V. J. Koester, J. Chem. Phys. **70**, 622 (1979).

[16] J. G. de la Torre, B. Carrasco, and S. E. Harding, Eur. Biophys. J. **25**, 361 (1997).

[17] E. Frederiq and C. Houssier, *Electric Dichroism and Electric Birefringence* (Clarendon, Oxford, 1973)

[18] A. Bjørkøy, A. Elgsaeter, and A. Mikkelsen, Biophys. Chem. **72**, 247 (1998).

[19] W. A. Wegener, R. M. Dowben, and V. J. Koester, J. Chem. Phys. **73**, 4086 (1980).

[20] R. B. Bird, C. F. Curtiss, R. C. Armstrong, and O. Hassager, *Dynamics of Polymeric Liquids*, 2nd ed. (Wiley, New York, 1987) Vol. 2.

[21] T. Nicolay and S. Cocard, Langmuir **16**, 8189 (2000).

[22] A. Mourchid and P. Levitz, Phys. Rev. E **57**, R4887 (1998); A. Knaebel, M. Bellour, J.-P. Munch, V. Viasnoff, F. Lequeux, and J. L. Harden, Europhys. Lett. **52**, 73 (2000).

[23] J. R. Van Wazer, J. W. Lyons, K. Y. Kim, and R. E. Colwell, *Viscosity and Flow Measurement-A Laboratory Handbook of Rheology* (Interscience, New York, 1963), Chap. 2.

[24] A. Bakk, M.Sc. project, NTNU, 1998.

[25] A. Bjørkøy, Ph.D. thesis, Norwegian University of Science and Technology, NTNU, 1997.

[26] R. G. Avery and J. D. F. Ramsay, J. Colloid Interface Sci. **109**, 448 (1986).
[27] L. Rosta and H. R. von Gunten, J. Colloid Interface Sci. **134**, 397 (1990).
[28] J. C. Bacri, R. Perzynski, D. Salin, V. Cabuil, and R. Massart, J. Magn. Magn. Mater. **62**, 36 (1986).
[29] A. O. Ivanov, Colloid J. USSR **59**, 446 (1997) [Kolloidnyi Zhurnal, **59**, 482 (1997)].